Asian Journal of Chemistry; Vol. 35, No. 6 (2023), 1423-1428

ASIAN JOURNAL OF CHEMISTRY

https://doi.org/10.14233/ajchem.2023.27810

Tailoring the Mechanistic Pathways and Kinetics of Decomposition of $CH_3CH_2C(O)OCH_2CH_2O$ Radical: A DFT Study

NABAM TAYUM[1], NAND KISHOR GOUR[2], ARUMUGAM MURUGAN[1,*] and BHUPESH KUMAR MISHRA[3,*]

[1]Department of Chemistry, North-Eastern Regional Institute of Science and Technology, Nirjuli-791109, India
[2]Department of Chemical Sciences, Tezpur University, Tezpur-784028, India
[3]Department of Chemistry, Dera Natung Government College, Itanagar-791113, India

*Corresponding authors: E-mail: amu@nerist.ac.in; bhupesh_chem@rediffmail.com

Received: 31 March 2023; *Accepted*: 25 April 2023; *Published online*: 27 May 2023; AJC-21258

The potential energy surface (PES) of the oxidative pathways and unimolecular decomposition of $CH_3CH_2C(O)OCH_2CH_2O$ radical formed from ethyl propionate has been investigated in details using *ab initio* density functional method. In present study, it is revealed that five major decomposition pathways with their kinetic and thermodynamics parameters. The geometries of reactants, transition states and product radicals were optimized using the model DFT method M06-2X along with the 6-31+G(d,p) basis set. The mechanistic, kinetic and thermochemical analysis was carried out at the M06-2X/aug-cc-pVTZ//M06-2X/6-311++G(d,p) level. Based on present results, it can be concluded that the oxidative pathway is the most significant for decomposition of $CH_3CH_2C(O)OCH_2CH_2O$ radical. The rate coefficients for each reaction channels were determined in a wide range of temperature 250-450 K.

Keywords: Biodiesel, Ethyl propionate, Alkoxy radical, α-Ester rearrangement.

INTRODUCTION

During past decade, it has been globally recognized that biodiesels can be used as a substitute of diesel fuels since they have same physical properties and concerns about climate change [1-3]. These are mainly derived from vegetable oils or animal fats *via* the transesterification process. The widespread use of fatty acid alkyl esters in diesel blends will lead to their release into the atmosphere. Ethyl propionate [$CH_3CH_2C(O)OCH_2CH_3$] is a model for studying the fatty acid ethyl esters which are used as first-generation biodiesel. Andersen *et al.* [4] reported the atmospheric oxidation of ethyl propionate for the first time and elucidated the fate of $CH_3CH_2C(O)OCH_2CH_2O$ radical considering three competing degradation pathways including oxidative pathways to form $CH_3CH_2C(O)OCH_2CHO$ and HO_2, α-ester rearrangement to produce propionic acid and decomposition to produce $CH_3CH_2C(O)OCH_2$ and CH_2O. In order to know the relative importance of each of these competing pathways, the atmospheric fate of $CH_3CH_2C(O)OCH_2CH_2O$ radical is needed. To date, the theoretical calculations to explore degradation of $CH_3CH_2C(O)OCH_2CH_2O$ radical, which have not been reported so far. This motivated us to perform a comprehensive investigation on the decomposition pathways of this radical.

The main objective of the present study is to investigate the complete reaction mechanism and kinetics of decomposition pathways of the alkoxy radical derived from ethyl propionate. Thus, the quantum chemical computations on the thermal unimolecular degradations and oxidative pathways of $CH_3CH_2C(O)OCH_2CH_2O$ radical were conducted. Five competing degradation reaction pathways involving oxidative pathways, α-ester rearrangement and thermal decomposition of $CH_3CH_2C(O)OCH_2CH_2O$ radical were taken into consideration to determine the end product formation. These atmospheric loss processes may take place potentially by the following reaction channels:

$$CH_3CH_2C(O)OCH_2CH_2O + O_2 \longrightarrow CH_3CH_2C(O)OCH_2CHO + HO_2 \quad (1)$$

$$\longrightarrow CH_3CH_2C(O)OH + CH_2CHO \quad (2)$$

$$\longrightarrow CH_3CH_2C(O)OCH_2 + CH_2O \quad (3)$$

$$\longrightarrow CH_3CH_2C(O)OCH_2CHO + H \quad (4)$$

$$\longrightarrow CH_3CH_2C(O)O + CH_2CH_2O \quad (5)$$

Alkoxy radicals are a key component in both the atmospheric and combustion oxidation pathways of volatile organic comp-

ounds. It is believed that these alkoxy radicals degrade *via* oxidative pathways (reaction with O_2), unimolecular decomposition reactions or isomerization. In recent years, alkoxy radicals have drawn the attention of the scientific community from both experimental and theoretical chemists [5-15], since it is inevitably responsible for the determination of the nature of the end-products of the oxidation of hydrocarbon in atmosphere. Reisi-Vanani & Hoseinpour [16] reported the fate of $C_3F_7OCH_2O$ radical derived from HFE-7000 using B3LYP and B3PW91 methods and based on his result, it was emphasized that oxidative pathways is the main degradation pathways of this radical in atmosphere.

In another study, Orlando [17] reported the atmospheric fate of C_2H_5-O-CH(O)CH_3 radical derived from diethyl ether and concluded that the dominant pathway of this radical is *via* C-C bond fission. Ferenac *et al.* [18] performed computational studies on oxygenated alkoxy radicals considering the unimolecular isomerization and decomposition. Based on theoretical study, it has been established that oxidative pathways will be the main degradation pathways for $CH_3CH_2OCH_2O$ and CH_3C-(O)CH_2CH_2O radicals. Similarly, Somnitz & Zellner [19] explored for the unimolecular reaction pathways of 1-butoxyl and 2-pentoxyl radicals, which can undergo 1,5 H-shift isomerization reactions. Somnitz & Zellner [20], in another study, reported the theoretical studies of unimolecular reactions of ethoxy, 1-butoxy, 2-butoxy and 2-pentoxy radicals considering C-C bond decomposition and isomerization reactions. Zhao *et al.* [21] performed kinetic study for the chlorine initiated oxidation of ethyl format at B3LYP/6-31G(d,p) level. The α-ester rearrangement and oxidation are the competitive path-ways for alkoxy radical HC(O)OCH(O)CH_3. Rayez *et al.* [22] also computed the barrier height to be 6.1 and 13.5 kcal mol^{-1}, respectively for CH_3C(O)OCH(O)CH_3 radical at B3LYP/6-31G (d,p) level for two competing pathways. In previous study [23], high-level *ab initio* methods have been employed to obtain the potential energy surface of CF_3C(O)OCH(O)CF_3 radical. Rate coefficients of the reaction channels were evaluated using canonical transition state theory to develop a kinetic model. The present work deals the first determination of rate coefficients and to evaluate the atmospheric degradation of radical by using sophisticated theoretical tools.

COMPUTATIONAL METHODS

All the calculations were performed using the Gaussian 09 [24] quantum chemistry software. The electronic structure properties of the reactants, products and the transition states involved in the degradation channels were obtained at hybrid meta density functional theory M06-2X [25] employing 6-31 +G(d,p) basis set to map out reactions mechanisms and to compute vibrational frequencies. Previous studies [26-31] revealed that the M06-2X functional satisfactorily perform in acquiring thermo-kinetic data. The harmonic vibrational frequencies of stationary points were computed to verify the nature of intermediates and transition states, no imaginary frequency individual local minima, one imaginary frequency individual transition states. The zero-point vibrational energy contributions have been considered in the calculation of energy barrier. In order to get the minimum energy path and to validate the connection between the transition states and designed reactants and products, IRC calculations were also performed [32] at M06-2X/6-31+G(d,p) level. To improve the accuracy of relative energy, a single point energy calculation of species using aug-cc-pVTZ basis set in the well-optimized geometry at the M06-2X/6-31 +G(d,p) level were also performed.

RESULTS AND DISCUSSION

Thermodynamic data: Thermodynamic calculations for reaction enthalpies ($\Delta_rH°$) and free energies ($\Delta_rG°$) at 298 K for atmospheric loss processes (1-5) performed at M06-2X/6-31+G(d,p) level are recorded in Table-1. The calculated $\Delta_rH°$ and $\Delta_rG°$ values suggested the spontaneity and feasibility of the decomposition pathways considered in present study. Based on Table-1, three reactions are possible due to being exergonic ($\Delta G < 0$). The results also revealed that pathways 4 and 5 is endoergic at 298 K; $\Delta_rH°$ = 18.53 and 92.01 kcal mol^{-1}, respectively and endergonic ($\Delta G > 0$) with 7.88 and 76.16 kcal mol^{-1}, respectively. Therefore, it can be assumed that reactions 4 and 5 are less important decomposition channels for radical.

TABLE-1
THERMOCHEMICAL DATA FOR REACTION CHANNELS (1-5) CALCULATED AT M06-2X/6-31+G(d,p) LEVEL OF THEORY

Reaction channels	$\Delta_rH°$ (kcal mol^{-1})	$\Delta_rG°$ (kcal mol^{-1})
Reaction 1 (reaction with O_2)	-29.54	-33.71
Reaction 2 (α-rearrangement)	-10.54	-24.71
Reaction 3 (C–C bond scission)	11.93	-2.60
Reaction 4 (C–H bond scission)	18.53	7.88
Reaction 5 (C–O bond scission)	92.01	76.16

Structural characteristics of transition states: Fig. 1 depicts the electronic structure of reactant, products and transition states optimized at the M06-2X/6-31+G(d,p) level. Transition states were optimized on relaxed potential energy surface, which are designated as TS1, TS2, TS3, TS4 and TS5, respectively. The results obtained from harmonic vibrational frequencies calculation at M06-2X/6-31+G(d,p) level are shown in Table-2. Analysis of the harmonic vibrational frequency of minima showed no imaginary frequency (NIMAG = 0), while each transition state has one imaginary frequency resulting from its first order saddle point character. For oxidative pathway reaction channel (1), the imaginary frequency of TS1 is -2603 cm^{-1} which correspond to O18-H15 and C14-H15 stretching mode also indicates the strong curvature in the potential energy surface (PES) around the transition state. For the α-ester rearrangement pathway involving TS2, the imaginary frequency was found to be -1294 cm^{-1}, which correspond to O4-H13 and H13-C12 stretching mode for hydrogen transfer reaction. The transition states TS3, TS4 and TS5 were optimized with one imaginary frequency obtained at -376, -924 and -653 cm^{-1} at M06-2X/6-31+G(d,p) level. The results obtained during IRC calculations [32] as shown in Figs. 2 and 3 further confirm that the transition state really connects the desired reactant and product along corresponding potential energy surface.

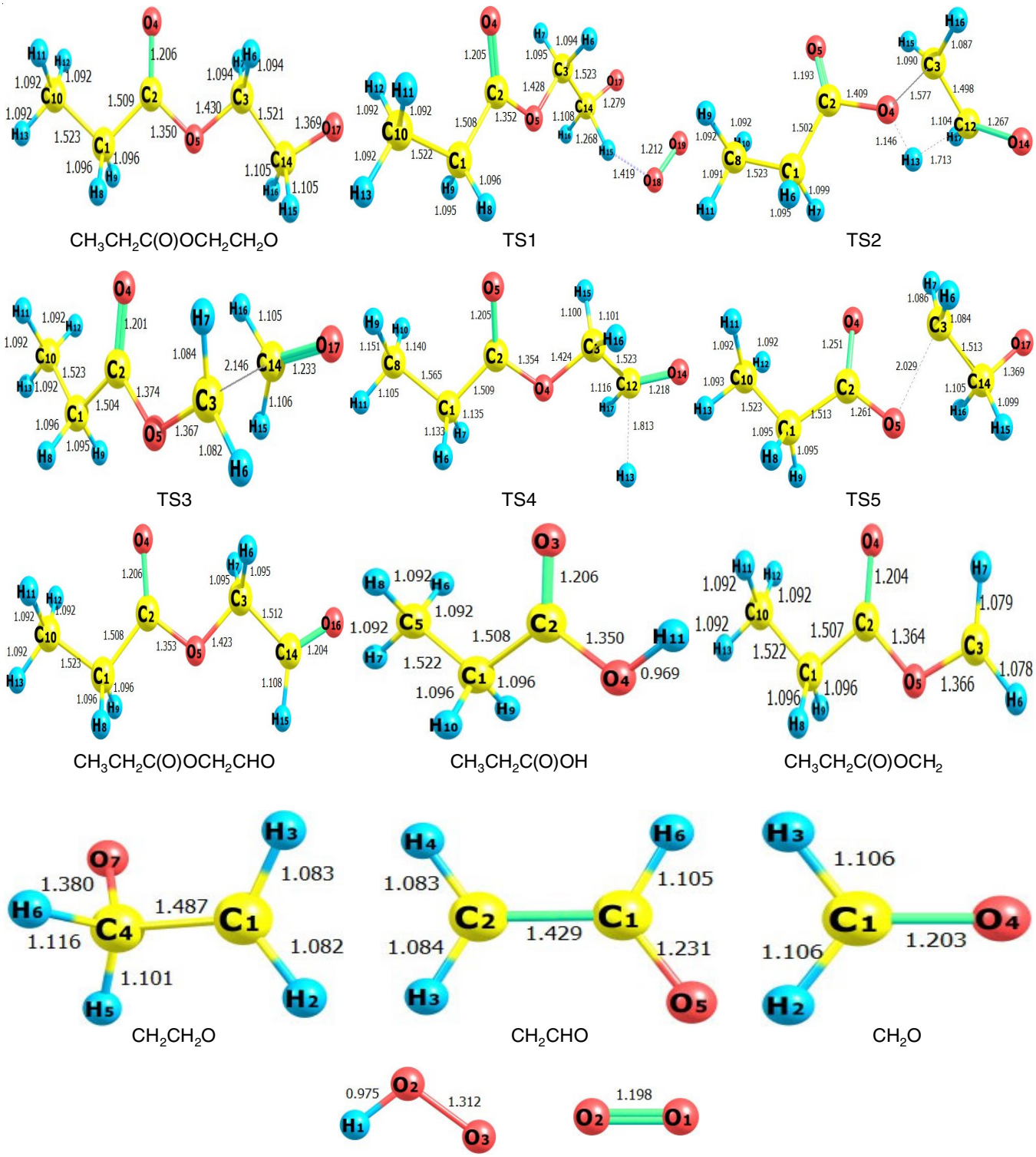

Fig. 1. Optimized geometries of reactants, transition states and products obtained at M06-2X/6-31+G(d,p). Bond lengths are in angstroms

In the most stable geometry of alkoxy radical, the C14-O17 bond length was found to be 1.32 Å, while the C2-O5 and C3-O5 bond lengths were found to be 1.350 and 1.430 Å, respectively. The two C-C bond distances labelled as C1-C2 and C3-C4, are also somewhat different (1.509 Å and 1.521 Å). Similarly, the C14-H14 bond (1.105 Å) is the longest one in comparison to 1.092 Å for all the other C-H bonds. For the oxidative pathways (reaction channel 1), the located transition state (TS1) as shown in Fig. 1 reveals the elongation of C-H (C14-H15) bond length from 1.105 to 1.268 Å (14.75 %) at the M06-2X level. The forming H15···O18 bond at the transition point was found to be 1.419 Å. The α-ester rearrangement pathway can be accomplished *via* intramolecular H-atom abstraction from carbon *via* the five-membered ring transition state TS2. During the transition, it is also observed that the forming O-H bond length (O4-H13) was found to be 1.146 Å along

TABLE-2
HARMONIC VIBRATIONAL FREQUENCIES OF REACTANTS, TRANSITION STATES AND PRODUCTS AT M06-2X/6-31+G(d,p) LEVEL OF THEORY

Species	Vibrational frequencies (cm^{-1})
$C_2H_5C(O)OCH_2CH_2O$	109, 144. 192, 222, 269, 292, 326, 378, 404, 544, 636, 687, 820, 874, 899, 987, 1018, 1034, 1078, 1089, 1118, 1141, 1215, 1252, 1301, 1307, 1343, 1399, 1417, 1445, 1455, 1494, 1512, 1529, 1551, 1848, 2812, 2828, 2904, 2916, 2929, 2943, 2966, 2983, 3124
TS1	2603i, 36, 90, 160, 194, 205, 244, 265, 332, 355, 396, 433, 458, 527, 564, 574, 603, 678, 730, 803, 852, 928, 948, 967, 1075, 1098, 1110, 1179, 1185, 1200, 1222, 1273, 1350, 1444, 1448, 1486, 1495, 1516, 1529, 1541, 1556, 1628, 1875, 2200, 2308, 2414, 2828, 2853, 2909, 2942, 2949
TS2	1294i, 61, 83, 95, 125, 187, 232, 264, 354, 442, 497, 562, 641, 676, 803, 819, 853, 928, 985, 1017, 1082, 1101, 1116, 1125, 1171, 1236, 1284, 1345, 1384, 1431, 1445, 1467, 1487, 1505, 1510, 1661, 1921, 3012, 3067, 3091, 3118, 3158, 3173, 3180, 3259
TS3	376i, 48, 54, 60, 83, 202, 219, 239, 305, 359, 476, 558, 580, 652, 694, 811, 864, 944, 1018, 1094, 1110, 1126, 1158, 1215, 1245, 1254, 1279, 1394, 1430, 1467, 1472, 1498, 1503, 1509, 1656, 1888, 2955, 3029, 3083, 3089, 3121, 3170, 3180, 3322
TS4	924i, 76, 119, 144, 201, 272, 308, 333, 390, 462, 494, 548, 574, 645, 717, 834, 912, 931, 971, 1078, 1094, 1122, 1133, 1172, 1250, 1265, 1318, 1351, 1406, 1440, 1468, 1499, 1505, 1522, 1543, 1762, 1871, 2647, 2736, 2766, 2802, 2914, 3029, 3041, 3096
TS5	653i, 40, 55, 127, 150, 193, 228, 272, 322, 502, 556, 601, 634, 669, 815, 848, 944, 1011, 1039, 1074, 1089, 1113, 1117, 1203, 1241, 1284, 1331, 1344, 1384, 1427, 1466, 1486, 1503, 1505, 1550, 1654, 3003, 3074, 3084, 3087, 3127, 3163, 3171, 3185, 3295
$C_2H_5C(O)OCH_2CHO$	27, 53, 65, 120, 157, 227, 266, 333, 399, 576, 588, 677, 733, 812, 913, 1024, 1075, 1090, 1109, 1113, 1135, 1250, 1252, 1280, 1346, 1402, 1420, 1433, 1469, 1482, 1503, 1509, 1871, 1889, 2997, 3084, 3089, 3090, 3123, 3140, 3170, 3172
HO_2	1268, 1459, 3713
$C_2H_5C(O)OH$	66, 222, 256, 473, 507, 624, 636, 811, 839, 1023, 1108, 1113, 1196, 1281, 1307, 1419, 1442, 1471, 1506, 1511, 1881, 3084, 3088, 3124, 3169, 3173, 3823
$CH_2CH(O)$	486, 512, 772, 981, 985, 1172, 1406, 1488, 1639, 3034, 3206, 3326
$C_2H_5C(O)OCH_2$	47, 164, 219, 226, 285, 362, 398, 462, 574, 664, 806, 863, 1019, 1095, 1108, 1161, 1198, 1278, 1280, 1396, 1430, 1456, 1470, 1505, 1510, 1875, 3082, 3086, 3121, 3167, 3171, 3216, 3370
HCHO	1212, 1275, 1547, 1881, 2977, 3050
$C_2H_5C(O)O$	62, 222, 244, 357, 474, 580, 798, 810, 990, 1083, 1104, 1262, 1305, 1342, 1431, 1466, 1506, 1512, 1763, 3080, 3088, 3143, 3161, 3165
CH_2CH_2O	184, 425, 502, 771, 928, 1086, 1095, 1157, 1366, 1381, 1460, 2865, 3038, 3203, 3320
O_2	1776

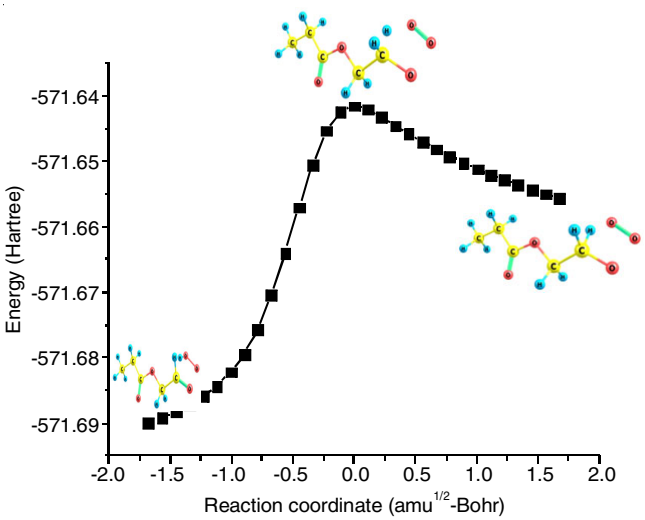

Fig. 2. IRC plot performed for transition states TS1 for oxidative pathways (reaction channel 1) of $CH_3CH_2C(O)OCH_2CH_2O$ radical

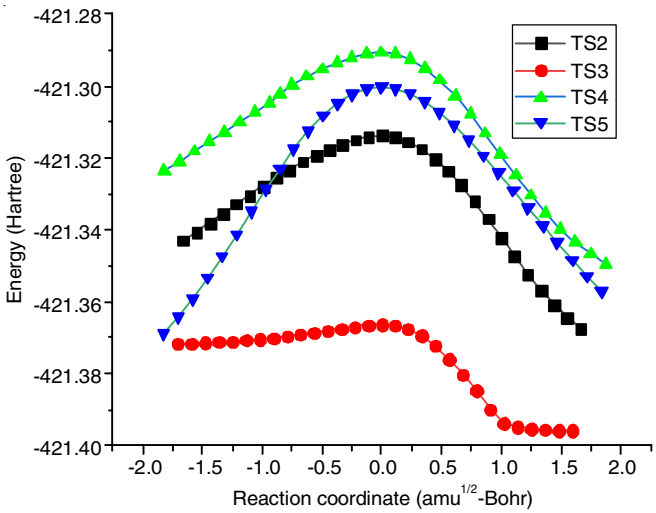

Fig. 3. IRC plots performed for transition states TS2, TS3, TS4 and TS5 obtained during thermal decomposition pathways of $CH_3CH_2C(O)OCH_2CH_2O$ radical

with elongation of C12-H13 bond from 1.105 to 1.713 Å (55%) and C3-O4 is strengthened up to 1.577 Å. Inspection of the structure of transition state (TS3) for reaction channel 3, the breaking of the C3-C14 bond is accomplished by stretching of 41.09% (1.521 to 2.146 Å), while the C14-O17 bond is decreased by 9.93% (1.369 to 1.233 Å) as compared to the reactants. Likewise, in TS4 the broken C - H (C12 -H13) bond stretched by 64.07% (1.105 to 1.813 Å) while the formed C-O (C12-O14) bond is decreased from 1.369 to 1.218 Å (11.02%). Similarly, for TS5 which results the formation of $CH_3CH_2C(O)O$ and CH_2CH_2O radicals, the broken C-O (C3-O5) is elongated from 1.430 to 2.029 Å (41.88%).

Energetics: Single point energy calculations for all the stationary state species involved in reaction channels obtained

from both the levels M06-2X/6-311++G(d,p) and M06-2X/aug-cc-pVTZ are summarized in Table-3. For energetic calculation, we have used M06-2X/6-31+G(d,p) optimized geometries of species. The zero-point energy of each species was determined from frequency calculation data performed at M06-2X/6-31+G(d,p) level of theory at which optimization was done and zero-point corrected total energies were determined with a scale factor of 0.967.

TABLE-3
CALCULATED ENERGY BARRIERS (kcal mol^{-1}) AT DIFFERENT LEVEL OF THEORIES

Reaction channels	M06-2X/aug-cc-pVTZ-	M06-2X/6-311++G(d,p)	M06-2X/6-31+G(d,p)
TS1 (reaction with O_2)	5.16	6.04	6.32
TS2 (α-rearrangement)	41.93	42.78	43.60
TS3 (C–C bond scission)	10.33	11.63	12.94
TS4 (C–H bond scission)	23.95	24.54	25.08
TS5 (C–O bond scission)	53.58	54.73	54.93

The associated energy barriers corresponding to reactions (1-5) calculated at different levels is recorded in Table-3. The barrier heights calculated at the M06-2X/aug-cc-pVTZ level amount to 5.16, 41.9, 10.33, 23.95 and 53.58 kcal mol^{-1} for TS1, TS2, TS3, TS4 and TS5, respectively. Whereas, the barrier heights for the same calculated as 6.04, 42.7, 11. 6, 24.5 and 54.7 kcal mol^{-1} at the M06-2X/6-311++G(d,p) level. It is observed that energy barrier decreases as the basis set is extended. This corroborates the dominance of oxidative pathways in the decomposition process of $CH_3CH_2C(O)OCH_2CH_2O$ radical. A schematic potential energy profile of the unimolecular decomposition and reactivity of alkoxy radical obtained at the M06-2X/aug-cc-pVTZ level with zero-point energy (ZPE) corrections is plotted in Fig. 4. In the construction of energy diagram, zero-point energy corrected total energy have been utilized. These energies are plotted with respect to the ground state energy of $CH_3CH_2C(O)OCH_2CH_2O//CH_3CH_2C(O)OCH_2CH_2O + O_2$ including ZPE arbitrarily taken as zero. Due to lack of experimental or theoretical data it is not possible to compare present results for decomposition channels of $CH_3CH_2C(O)OCH_2CH_2O$ radical.

Based on the energetic calculations, it is worth mentioning that among the investigated reaction channels, oxidation pathway (reaction with O_2) is the most significant decomposition pathway for $CH_3CH_2C(O)OCH_2CH_2O$ radical. This is in line with the previously proposed findings of Picquet-Varrault *et al.* [9] for $CH_3C(O)OCH_2CH_2CH_2O$ radical and $HC(O)OCH_2O$

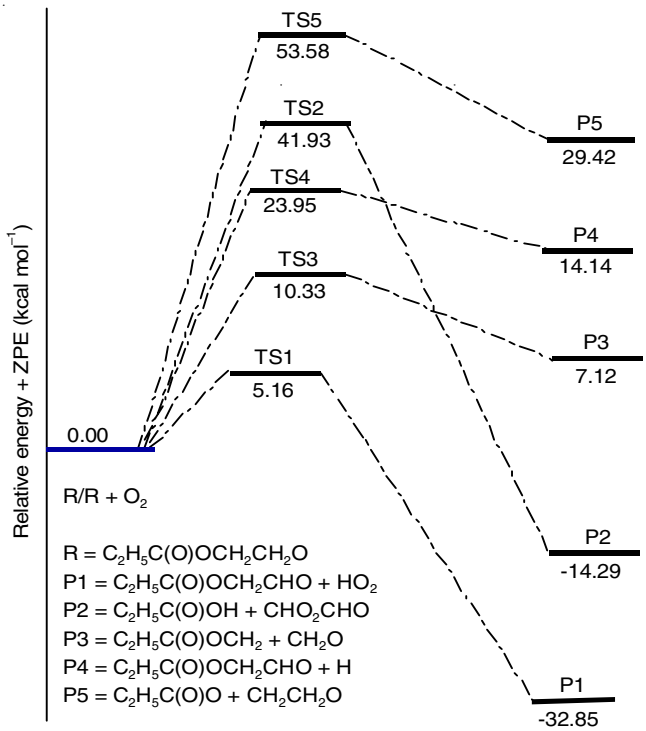

Fig. 4. Relative energy diagram for the oxidative and thermal decomposition pathways of $CH_3CH_2C(O)OCH_2CH_2O$ radical at M06-2X/aug-cc-pVTZ level of theory

reported by Wallington *et al.* [33]. Present findings in this study also supports the conclusions made by Wallington *et al.* [7] and Ninomiya *et al.* [5] regarding the fate of $C_4F_9OCH_2O^{\bullet}$ and $n\text{-}C_3F_7OCH_2O^{\bullet}$ radicals along with other theoretical studies [12-16] performed for other similar alkoxy radicals.

Kinetics calculation: The rate coefficient values for different reaction channels were computed by using the conventional transition state theory (CTST) [34] and incorporating Eckart's tunneling correction [35,36] over the temperature range of 250-450 K by using the following expression:

$$k = \Gamma(T)\frac{k_b T}{h}\frac{Q^{\ddagger}_{TS}}{Q_R}\exp\frac{-\Delta E}{RT} \quad (6)$$

The discussion about the rate coefficient calculation is provided in previous studies [23,26]. In present work, the kinetic rate coefficients for reaction pathways (1-5) were performed by means of the kinetic and statistical thermodynamical package (KiSThelP) programme [37]. The obtained rate coefficients in the temperature range of 250-450 K for reaction pathways (1-5) are depicted in Table-4. At 298 K, the calculated rate

TABLE-4
CALCULATED RATE CONSTANTS FOR FIVE DECOMPOSITION PATHWAYS IN TEMPERATURE RANGE 250-450 K AT M06-2X/aug-cc-pVTZ LEVEL

	TS1	TS2	TS3	TS4	TS5
250	2.70×10^{-17}	9.01×10^{-23}	1.18×10^{3}	7.91×10^{-9}	1.05×10^{-34}
298	1.12×10^{-16}	1.13×10^{-17}	1.15×10^{5}	1.86×10^{-5}	6.47×10^{-27}
300	1.18×10^{-16}	1.77×10^{-17}	1.36×10^{5}	2.44×10^{-5}	1.20×10^{-26}
350	4.03×10^{-16}	3.07×10^{-13}	4.27×10^{6}	8.93×10^{-3}	7.39×10^{-21}
400	1.13×10^{-15}	6.28×10^{-10}	5.89×10^{7}	8.04×10^{-1}	1.68×10^{-16}
450	2.75×10^{-15}	2.65×10^{-7}	4.66×10^{8}	2.78×10^{1}	4.26×10^{-13}

The unit of rate constant is s^{-1} except for TS1 which is in cm^3 $molecule^{-1}$ s^{-1}

constants for TS1 and TS2 were found to be 1.12×10^{-16} cm^{-3} mol^{-1} s^{-1} and 1.13×10^{-17} s^{-1}, respectively at M06-2X//aug-cc-pVTZ level of theory. Similarly, for TS3, TS4 and TS5, the calculated rate coefficients were found to be 1.15×10^{5}, 1.86×10^{-5} and 6.47×10^{-27} s^{-1}, respectively at 298 K and 1 atm. Unfortunately, we were unable to compare the present computed values from this study to any existing experimental or theoretical evidence in the literature. Due to scarcity of experimental or theoretical data, it is expected that the results may be helpful for future laboratory investigations.

Conclusion

A theoretical study was performed on the degradation of $CH_3CH_2C(O)OCH_2CH_2O$ radical using a combination of DFT method M06-2X/6-31+G(d,p) and energetic calculations were performed at M06-2X/aug-cc-pVTZ method. Five reaction channels were identified and taken in consideration for details study. The calculated energy barriers for the channels (1), (2), (3), (4) and (5) obtained were 5.16, 41.93, 10.33, 23.95 and 53.58 kcal mol^{-1}, respectively at M06-2X/aug-cc-pVTZ level of theory. The potential energy profile diagram and thermochemistry investigation revealed that reaction with O_2 is the main degradation process for $CH_3CH_2C(O)OCH_2CH_2O$ radical. This conclusion is in line with the experimental and theoretical studies for other structurally similar alkoxy radicals. The kinetic models were developed along with detailed mechanism pathways to underpin the dissociation of radical in atmosphere. The reaction rate coefficients were computed by employing the canonical transition state theory and the value of the rate constant for the most dominant oxidative pathways was estimated as 1.12×10^{-16} cm^{-3} mol^{-1} s^{-1} at 298 K using M06-2X//aug-cc-pVTZ level.

ACKNOWLEDGEMENTS

One of the authors, Nabam Tayum is thankful to Ministry of Tribal Affairs, Government of India for providing the National Fellowship & Scholarship for Higher Studies (Award No: 202122-NFST-ARU-00279).

CONFLICT OF INTEREST

The authors declare that there is no conflict of interests regarding the publication of this article.

REFERENCES

1. J.Y.W. Lai, K.C. Lin and A. Violi, *Pror. Energy Combust. Sci.*, **37**, 1 (2011); https://doi.org/10.1016/j.pecs.2010.03.001
2. A. Demirbas, *Energy Policy*, **35**, 4661 (2007); https://doi.org/10.1016/j.enpol.2007.04.003
3. W. Li, J. Li, H. Ning, Y. Shang and S.N. Luo, *J. Phys. Chem. A*, **125**, 5103 (2021); https://doi.org/10.1021/acs.jpca.1c01788
4. V.F. Andersen, K.B. Ørnsø, S. Jørgensen, O.J. Nielsen and M.S. Johnson, *J. Phys. Chem. A*, **116**, 5164 (2012); https://doi.org/10.1021/jp300897t
5. Y. Ninomiya, M. Kawasaki, A. Guschin, L.T. Molina, M.J. Molina and T.J. Wallington, *Environ. Sci. Technol.*, **34**, 2973 (2000); https://doi.org/10.1021/es991449z
6. L.K. Christensen, J.C. Ball and T.J. Wallington, *J. Phys. Chem. A*, **104**, 345 (2000); https://doi.org/10.1021/jp993127n
7. T.J. Wallington, W.F. Schneider, J. Sehested, M. Bilde, J. Platz, O.J. Nielsen, L.K. Christensen, M.J. Molina, L.T. Molina and P.W. Wooldridge, *J. Phys. Chem. A*, **101**, 8264 (1997); https://doi.org/10.1021/jp971353w
8. J.J. Orlando and G.S. Tyndall, *Int. J. Chem. Kinet.*, **42**, 397 (2010); https://doi.org/10.1002/kin.20493
9. B. Picquet-Varrault, J.F. Doussin, R. Durand-Jolibois and P. Carlier, *Phys. Chem. Chem. Phys.*, **3**, 2595 (2001); https://doi.org/10.1039/b101704g
10. J.J. Orlando, G.S. Tyndall and T.J. Wallington, *Chem. Rev.*, **103**, 4657 (2003); https://doi.org/10.1021/cr020527p
11. L. Vereecken and J.S. Francisco, *Chem. Soc. Rev.*, **41**, 6259 (2012); https://doi.org/10.1039/c2cs35070j
12. B.K. Mishra, M. Lily, R.C. Deka and A.K. Chandra, *New J. Chem.*, **40**, 6148 (2016); https://doi.org/10.1039/C5NJ02752G
13. D. Bhattacharjee, B.K. Mishra and R.C. Deka, *J. Mol. Model.*, **21**, 69 (2015); https://doi.org/10.1007/s00894-015-2629-x
14. B.K. Mishra, N.K. Gour, D. Bhattacharjee and R.C. Deka, *Mol. Phys.*, **114**, 618 (2016); https://doi.org/10.1080/00268976.2015.1108471
15. B.K. Mishra, M. Lily, R.C. Deka and A.K. Chandra, *J. Mol. Graph. Model.*, **50**, 90 (2014); https://doi.org/10.1016/j.jmgm.2014.03.009
16. A. Reisi-Vanani and S. Hoseinpour, *Arab. J. Chem.*, **10**, S1604 (2017); https://doi.org/10.1016/j.arabjc.2013.05.030
17. J.J. Orlando, *Phys. Chem. Chem. Phys.*, **9**, 4189 (2007); https://doi.org/10.1039/b706819k
18. M.A. Ferenac, A.J. Davis, A.S. Holloway and T.S. Dibble, *J. Phys. Chem. A*, **107**, 63 (2003); https://doi.org/10.1021/jp0262923
19. H. Somnitz and R. Zellner, *Phys. Chem. Chem. Phys.*, **2**, 1907 (2000); https://doi.org/10.1039/b000029i
20. H. Somnitz and R. Zellner, *Phys. Chem. Chem. Phys.*, **2**, 1899 (2000); https://doi.org/10.1039/b000037j
21. Y. Zhao, X. Sun, W. Wang and L. Xu, *Can. J. Chem.*, **92**, 598 (2014); https://doi.org/10.1139/cjc-2014-0108
22. M.-T. Rayez, B. Picquet-Varrault, F. Caralp and J.-C. Rayez, *Phys. Chem. Chem. Phys.*, **4**, 5789 (2002); https://doi.org/10.1039/B207511N
23. B.K. Mishra, *RSC Adv.*, **4**, 16759 (2014); https://doi.org/10.1039/c4ra00881b
24. M.J. Frisch *et al.* Gaussian 09, Revision B.01; Gaussian, Inc.: Wallingford, CT, USA (2010).
25. Y. Zhao and D.G. Truhlar, *Theor. Chem. Acc.*, **120**, 215 (2008); https://doi.org/10.1007/s00214-007-0310-x
26. N.K. Gour, K. Borthakur, S. Paul and R.C. Deka, *Chemosphere*, **238**, 124556 (2020); https://doi.org/10.1016/j.chemosphere.2019.124556
27. M. Lily, B. Baidya and A.K. Chandra, *Chem. Phys. Lett.*, **669**, 211 (2017); https://doi.org/10.1016/j.cplett.2016.12.037
28. P.K. Rao, R.C. Deka, N.K. Gour and S.P. Gejji, *J. Phys. Chem. A*, **122**, 6799 (2018); https://doi.org/10.1021/acs.jpca.8b04225
29. B. Baidya, M. Lily, D. Patgiri, S. Hynniewta and A.K. Chandra, *New J. Chem.*, **44**, 4276 (2020); https://doi.org/10.1039/C9NJ06069C
30. S. Paul, B.K. Mishra, S.D. Baruah, R.C. Deka and N.K. Gour, *Environ. Sci. Pollut. Res. Int.*, **27**, 907 (2020); https://doi.org/10.1007/s11356-019-06975-1
31. N.K. Gour, B.K. Mishra, P.J. Sarma, P. Begum and R.C. Deka, *J. Fluor. Chem.*, **204**, 11 (2017); https://doi.org/10.1016/j.jfluchem.2017.09.010
32. C. Gonzalez and H.B. Schlegel, *J. Chem. Phys.*, **90**, 2154 (1989); https://doi.org/10.1063/1.456010
33. T.J. Wallington, M.D. Hurley, T. Maurer, I. Barnes, K.H. Becker, K.G.S. Tyndall, J.J. Orlando, A.S. Pimentel and M. Bilde, *J. Phys. Chem. A*, **105**, 5146 (2001); https://doi.org/10.1021/jp0041398
34. K.J. Laidler, Chemical Kinetics, Pearson Education, New Delhi, India, Edn 3 (2004).
35. H.S. Johnston and J. Heicklen, *J. Phys. Chem.*, **66**, 532 (1962); https://doi.org/10.1021/j100809a040
36. R. Xiao, M. Noerpel, H. Ling Luk, Z. Wei and R. Spinney, *Int. J. Quantum Chem.*, **114**, 74 (2014); https://doi.org/10.1002/qua.24518
37. S. Canneaux, F. Bohr and E. Henon, *J. Comput. Chem.*, **35**, 82 (2014); https://doi.org/10.1002/jcc.23470